Annealing-induced vacancy formation enables extraordinarily high Li^+ ion conductivity in the amorphous electrolyte 0.33 LiI + 0.67 Li_3PS_4

Stefan Spannenberger[a,1], Vanessa Miß[a,1], Edda Klotz[b], Janosch Kettner[a], Marvin Cronau[a], Asvitha Ramanayagam[a], Francesco di Capua[b], Mohamed Elsayed[c,d], Reinhard Krause-Rehberg[c], Michael Vogel[b], Bernhard Roling[a,*]

[a] Department of Chemistry, Philipps-Universität Marburg, Hans-Meerwein-Straße 4, D-35032 Marburg, Germany
[b] Institut für Festkörperphysik, Technische Universität Darmstadt, Hochschulstr. 6, D-64289 Darmstadt, Germany
[c] Institut für Physik, Martin-Luther-Universität Halle Wittenberg, Von-Danckelmann-Platz 3, D-06099 Halle (Saale), Germany
[d] Department of Physics, Faculty of Science, Minia University, 61519 Minia, Egypt

ABSTRACT

Lithium thiophosphate glasses and glass ceramics are a promising class of electrolytes for all-solid-state lithium-ion batteries. Heat treatment of completely amorphous glasses often leads to a conductivity enhancement, which can be attributed either to the formation of highly conducting crystallites or to fast Li^+ ion transport at the interface between amorphous phases and crystallites. Here, we demonstrate a novel conductivity enhancement mechanism in amorphous 0.33 LiI + 0.67 Li_3PS_4 glasses during a single annealing step at 180 °C. The combination of electrochemical impedance, ^7Li NMR, and positron-annihilation lifetime spectroscopy gives indication for an annealing-induced formation of monovacancies in the bulk amorphous phase, which act as stepping stones for fast Li^+ ion transport. The maximum conductivity achieved after annealing was 6.5 $mS \cdot cm^{-1}$, the highest value observed so far for amorphous thiophosphate-based electrolytes.

1. Introduction

All-solid-state batteries (ASSBs) hold great promise for becoming the next-generation energy source of electric vehicles [1–3]. As compared to state-of-the-art lithium-ion batteries containing flammable liquid electrolytes, ASSBs offer potentially higher energies densities due to the usage of Li metal as anode material and higher safety due to the non-flammability of many solid electrolytes. The recent discovery of a large number of solid Li^+ electrolytes with ionic conductivities in the range of 10–25 $mS \cdot cm^{-1}$ [1,4–8] has led to exciting new perspectives for the development of high-power ASSBs. A large fraction of these solid Li^+ electrolytes are thiophosphates with crystal structures favouring fast Li^+ ion transport [1,4–10]. However, the total Li^+ ion conductivity of such crystalline materials may suffer from grain boundary resistances, which can only be reduced by time-consuming annealing processes at relatively high temperatures [5]. An alternative are lithium thiophosphate (LPS) glasses, which can often be synthesized in a simple fashion, e.g. by mechanochemical ball milling [3,11]. The addition of lithium iodide to LPS glasses improves the ionic conductivity [12–14] and also the compatibility with metallic lithium anodes [15–19]. However, the best ionic conductivities achieved so far in completely amorphous lithium thiophosphate – lithium iodide (LPSI) glasses do not exceed 1.8 $mS \cdot cm^{-1}$ [18].

Heat treatment of such glasses can lead to significant conductivity enhancements which have been attributed to different origins: (i) The formation of superionic $Li_7P_3S_{11}$ crystals in the amorphous matrix [3,20–22]. (ii) The formation of a highly conductive thio-LISICON II phase in the amorphous matrix [14,23]. (iii) Fast ion transport at the interfaces between crystalline phase and the amorphous phase [24,25]. In all three cases, the enhancement is related to the formation of crystallites.

In this paper, we demonstrate a novel conductivity enhancement mechanism during heat treatment of LPSI glasses, which is neither based on highly conductive crystallites nor on fast interfacial ion transport, but is caused by faster ion transport in the bulk amorphous phase. We show that a simple one-step heat treatment of the glass 0.33 LiI + 0.67 Li_3PS_4, which was prepared by mechanochemical milling, leads to a conductivity enhancement from about 0.8 $mS \cdot cm^{-1}$ to 6.5 $mS \cdot cm^{-1}$ without significant crystallization of the glass. To the best of our knowledge, 6.5 $mS \cdot cm^{-1}$ is the highest Li^+-conductivity obtained so far in inorganic amorphous Li^+ ion conductors. By combining electrochemical impedance spectroscopy (EIS), ^7Li NMR measurements, and positron annihilation lifetime (PAL) spectroscopy, we provide evidence that the Li^+ conductivity enhancement is caused by the

---

* Corresponding author.
  E-mail address: roling@staff.uni-marburg.de (B. Roling).
[1] These authors contributed equally to this work.

annealing-induced formation of monovacancies in the amorphous bulk phase of the material.

2. Experimental section

The Li_2S-P_2S_5-LiI glasses were prepared by the means of mechanical milling using a high energy planetary ball mill (Pulverisette 7, Fritsch, Idar-Oberstein, Germany). A stoichiometric mixture of reagent grade Li_2S (99.9%, Alfa Aesar, Karlsruhe, Germany), P_2S_5 (99%, Sigma Aldrich, Taufkirchen, Germany) and LiI (99.999%, Alfa Aesar, Karlsruhe, Germany) powders was prepared inside an argon-filled glovebox (UniLab, MBraun, Garching, Germany; $x_{H2O} < 1\,ppm$, $x_{O2} < 1\,ppm$) and was filled into a zirkonia pot (20 ml volume) with 10 ZrO_2 balls (10 mm diameter). After closing the pot air-tight, it was removed from the glovebox, and the mixture was milled at a rotational speed of 500 rpm for about 8 h (5 min milling; 15 min rest; 99 cycles). Afterwards, the obtained product was removed from the pot inside the glovebox and was ground in an agate mortar to obtain the final glass-powder. Each annealing step of the glass comprised heating from 20 °C to 180 °C in 20 min, holding at 180 °C for 30 min, and cooling from 180 °C to 20 °C in 20 min. All further sample preparation processes were also carried out inside the glovebox.

For the Li^+ ion conductivity measurements, the as-prepared powders were pressed into pellets with a diameter of 6 mm by applying a pressure of 276 MPa for 30 min at room temperature by means of a hydraulic press (P/O/Weber, Remshalden, Germany) using polished stainless steel extrusion dies. The thickness of the pellets was determined by means of a micrometer caliper (Mitutoyo, Neuss, Germany). To ensure a sufficient electronic contact during the measurements, the pellets were coated with a gold layer on both faces using a sputter coater (108auto, Cressington, Watford, England). The pellets were then placed inside a home-built, air-tight sample cell in a two-electrode arrangement. Impedance measurements were carried out using an Alpha-AK impedance analyzer (Novocontrol, Montabaur, Germany) in a frequency range from 1 MHz to 0.1 Hz with an applied AC voltage of 10 mV_{RMS}. The temperature was varied in a range from −120 °C to 180 °C using the Novocontrol Quatro Cryosystem. The maximum temperature offset during the measurements was fixed to a limit of ± 1 °C. For the fitting of the obtained spectra, the impedance analysis software RelaxIS (RHD Instruments, Darmstadt, Germany) was used.

X-ray diffraction measurements (XRD) were performed using a powder diffractometer STOE STADI MP (STOE, Darmstadt, Germany) using Cu-Kα radiation in a Debye-Scherrer geometry. The powder samples were sealed inside a XRD glass sample tube (Hilgenberg, Malsfeld, Germany) under argon atmosphere.

For ^7Li NMR measurements, the powder samples were pressed into pellets with 3 mm diameter. The pellets were then sealed into NMR glass tubes (Sigma Aldrich, Taufkirchen, Germany) under vacuum. During the NMR measurements, the temperature was controlled by a liquid nitrogen cryostat in a range between −173 °C and 27 °C. All experiments in homogeneous fields were carried out using a home-built spectrometer operating at a magnetic field of $B_0 = 4.6\,T$, corresponding to a ^7Li Larmor frequency of $\omega_L = 2\pi \cdot 63\,MHz$. Spin-lattice relaxation (SLR) measurements as well as spectra were recorded with a saturation-recovery pulse sequence followed by solid-echo detection. In order to ensure proper excitation of the broad static spectra, the 90° pulse length was kept at 2.2–2.3 μs in all experiments. Correlation functions of the ion dynamics were measured by applying the stimulated-echo (STE) pulse sequence for spin 3/2 [26,27]. Diffusion coefficients were measured using a static field gradient (SFG) magnet with the same magnetic field strength of $B_0 = 4.6\,T$ and a magnetic field gradient of $g = 140\,T\cdot m^{-1}$. The STE pulse sequence applied for diffusion measurements can be found in previous work [28]. Due to the identical field strength, spin-lattice relaxation times for the diffusion measurements could be resumed from the homogeneous field data.
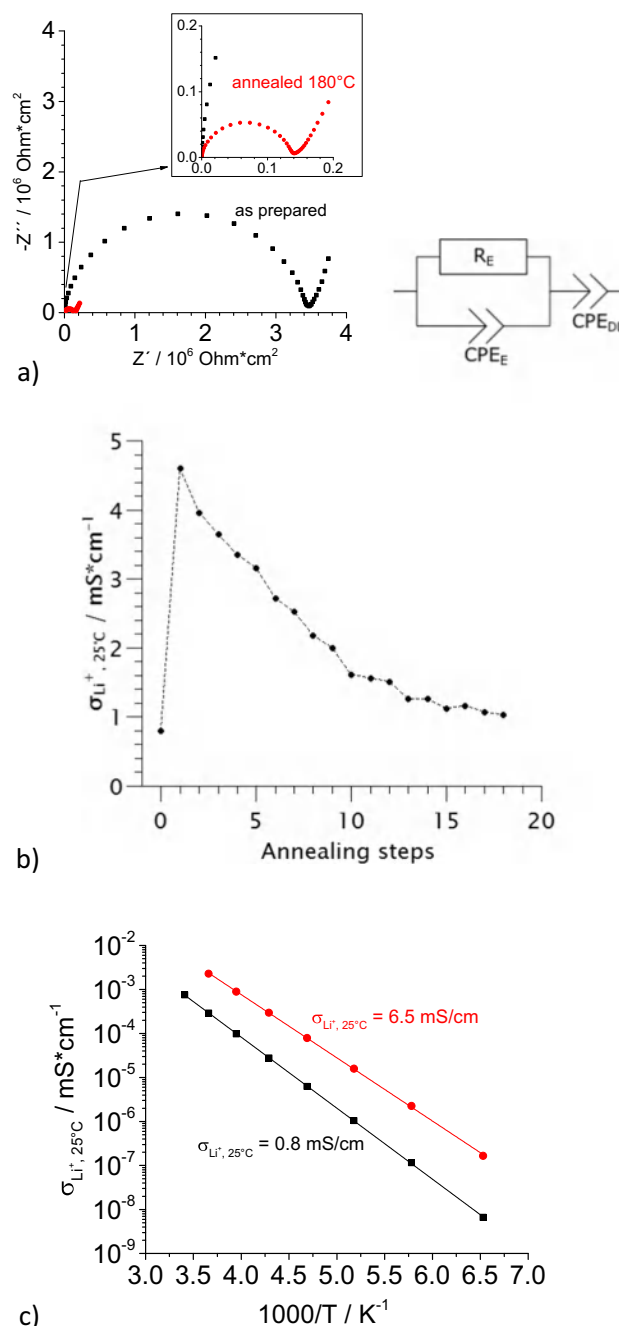

a)

b)

c)

Fig. 1. a) Nyquist plot of the complex impedance for the as-prepared 0.33 LiI + 0.67 Li_3PS_4 glass (black squares) and for the same sample after a single annealing step at 180 °C (red circles), respectively. The spectra were recorded at a temperature of −120 °C. On the right-hand side, the equivalent circuit used for fitting the impedance spectra is shown. b) Room-temperature Li^+ ion conductivity of the LiPSI glass versus the number of annealing steps implying an overall holding time of 9 h at 180 °C. c) Arrhenius plots of the ionic conductivity of the as-prepared glass (black squares) and of the same sample after a single annealing step (red circles). The solid lines represent the best linear fit. (For interpretation of the references to color in this figure legend, the reader is referred to the web version of this article.)

The positron annihilation lifetime (PAL) measurements were performed using a standard temperature-controlled digital positron lifetime spectrometer [29,30] with a time resolution of 228 ps. A 14 μCi ^{22}Na positron source was deposited between two 7.5 μm thick Kapton foils, which were sandwiched between two identical cylindrical as-prepared glass samples with 10 mm diameter and 1 mm thickness. The

measurements were carried out at room temperature (RT) under high vacuum ($< 10^{-6}$ mbar). Then the samples were annealed for 30 min at 180 °C, cooled down to room temperature, and were characterized again by PAL measurements. 5×10^6 counts were accumulated in each positron lifetime spectrum. Si was measured as a reference, which showed a single lifetime of 218 ps (defect-free bulk lifetime, τ_b). After source and background corrections, the lifetime spectra were decomposed two components, $n(t) = (I_1/\tau_1)e^{-t/\tau_1} + (I_2/\tau_2)e^{-t/\tau_2}$, convoluted with the Gaussian resolution function of the spectrometer using the lifetime program LT9 [31]. Here, I_i and τ_i denote the relative intensity and lifetime, respectively, of component i.

3. Results and discussion

In Fig. 1 a), we show impedance spectra obtained at -120 °C for the as-prepared glass and for the glass after a single annealing step. Both spectra were fitted with the equivalent circuit shown in Fig. 1 a). The semicircle was fitted by a resistance R_E in parallel to a constant phase element CPE_E, while the low-frequency spike due to electrode polarization (double layer formation) was fitted by a constant phase element CPE_{DL}. The impedance of a constant phase element is given by: $Z_{CPE} = Q^{-1} \cdot (i\omega)^{-\alpha}$. The capacitance of the semicircle can be calculated from the Brug formula $C_E = (Q_E \cdot (R_E)^{1-\alpha})^{1/\alpha}$ [32]. Capacitance values of 28 pF·cm^{-2} and 39 pF·cm^{-2} were obtained for the as-prepared and for the annealed glass, respectively, strongly indicating a bulk conduction process in both cases [33].

As seen from the figure, the one-step annealing leads to a strong increase of the bulk ion conductivity of the material. The room temperature ionic conductivity increases from 0.8 mS·cm^{-1} to 4.6 mS·cm^{-1}, see Fig. 1 b). However, longer-term annealing leads to a strong drop of the conductivity. After 18 annealing steps implying an overall holding time of 9 h at 180 °C, the room-temperature ionic conductivity drops to values of about 1 mS·cm^{-1}. We found no significant influence of the holding time at 180 °C (varied between 3 min and 30 min) and of the cooling rate (varied between 0.5 K·min^{-1} and 5 K·min^{-1}) on the conductivity enhancement.

Fig. 1 c) shows an Arrhenius plot of the ionic conductivity for the as prepared LiPSI glass (black squares) and for the same sample after the one-step annealing at 180 °C (red circles), respectively. The highest room-temperature ionic conductivity achieved by this one-step annealing was 6.5 mS·cm^{-1}, which is about eight higher than the conductivity of the as-prepared glass. We note that the maximum conductivity in subsequent experiments varied typically between 4.5 mS·cm^{-1} and 6.5 mS·cm^{-1}, even under nominally identical experimental conditions. The activation energy was lowered from 0.31 eV for the pristine glass to 0.28 eV for the annealed sample.

In Fig. 2, we show XRD patterns of the as-prepared glass, of a sample after a single annealing step leading to the maximum conductivity of 6.5 mS·cm^{-1}, and of a sample after 18 annealing steps (overall 9 h holding time at 180 °C) leading to a drop of the conductivity to 1 mS·cm^{-1}. The as-prepared sample is completely amorphous. The sample with the maximum Li$^+$ ion conductivity is mostly amorphous, but contains a tiny amount of crystalline phase as indicated by the weak Bragg peak at 19–21°. In contrast, after 18 annealing steps, the sample exhibits a much higher degree of crystallinity, and the largest Bragg peaks originate from Li$_4$PS$_4$I crystals, see XRD pattern of crystalline Li$_4$PS$_4$I in Fig. 2. Sedlmeyer et al. reported a value of 0.12 mS·cm^{-1} for the ionic conductivity of crystalline Li$_4$PS$_4$I [34]. Since Li$_4$PS$_4$I exhibits a higher iodide content than the as-prepared glass, we expect the simultaneous formation of Li$_3$PS$_4$. The XRD patters obtained after 18 annealing step do not show Bragg peaks originating from crystalline β-Li$_3$PS$_4$ or γ-Li$_3$PS$_4$ [35]. This indicates the formation of amorphous Li$_3$PS$_4$ with a room-temperature ionic conductivity of 0.124 mS·cm^{-1} [36]. Thus after very long time annealing, the conductivity data shown in Fig. 1 b) should approach a value of about 0.12 mS·cm^{-1}.

Since the Li$_4$PS$_4$I crystallites and amorphous Li$_3$PS$_4$ exhibit lower

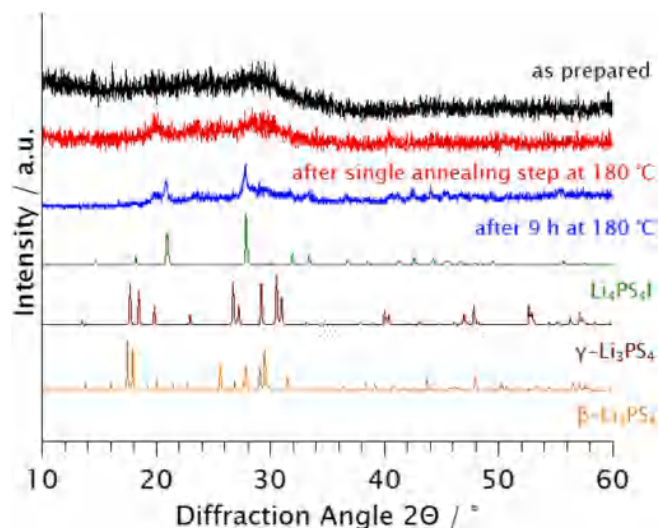**Fig. 2.** XRD pattern of the as prepared glass (σ = 0.8 mS·cm^{-1}), of the sample after a single annealing step (σ = 6.5 mS·cm^{-1}), of the sample after 18 annealing steps (σ = 1 mS·cm^{-1}), of crystalline Li$_4$PS$_4$I, of crystalline γ-Li$_3$PS$_4$ and of crystalline β-Li$_3$PS$_4$.

ionic conductivity than the as-prepared glass, it is remarkable that a short annealing step leads to a conductivity enhancement. Conductivity maxima during annealing close to the crystallization temperature have also been observed by Adams and Maier [37] for a Ag$^+$ ion conducting glass and by Tsukasaki et al. [24] and by Shiotani et al. [25] for Li$^+$ ion conducting glasses. In these studies, the conductivity enhancement was attributed to fast ion transport at the interfaces between the crystallites and the amorphous matrix. However, it is important to note that the maximum conductivity enhancements observed in these studies due to the interfacial effect was only about 80%, whereas we find a conductivity enhancement of up to 700%. Therefore, the question arises whether the origin of our conductivity enhancement is different.

In order to characterize the Li ion dynamics in more detail, we carried out ^{7}Li NMR experiments. These experiments probe the quadrupolar interactions of the ^{7}Li spins, which reflect the local charge distribution and, hence, differ at various ionic sites. Temperature-dependent ^{7}Li NMR spectra of the as-prepared glass and of a sample after a single annealing step are shown in Fig. 3 a). As expected for spin-3/2 nuclei [26], the static spectra at low temperatures consist of two Gaussian lines, which result from the central and satellite transitions between the Zeeman levels of the spins, respectively. The static width of the narrower central line amounts to $\Sigma_{centr} \approx 4$ kHz for both samples, whereas that of the broader satellite line changes upon annealing from $\Sigma_{sat} \approx 50$ kHz to $\Sigma_{sat} \approx 60$ kHz. The latter values reflect the fact that the ^{7}Li spins are subject to broadly distributed quadrupolar interactions in the studied disordered samples. When the temperature is increased, the NMR interactions responsible for the line broadening are averaged by Li motion, leading to line narrowing. At ambient temperatures, the ^{7}Li spectra are dominated by a narrow Lorentzian line, indicating that correlation times $\tau \leq 1$ μs prevail, but closer inspection reveals that a broader component still exists and, hence, the line-shape transition is not yet fully completed. Comparing the motional narrowing of the ^{7}Li spectra for the as-prepared glass and for the annealed samples, we find quantitative, but no qualitative differences. For a more detailed study, we show the temperature-dependent linewidth of the central line in Fig. 3 b). It can be seen that the line-shape transitions have similar shapes and extend over broad temperature ranges of > 100 K, suggesting prominent dynamical heterogeneity in both samples. In the case of heterogeneous dynamics, the temperature dependence of the line width depends on both the shift and width of the underlying distribution of correlation times, hampering straightforward determination of
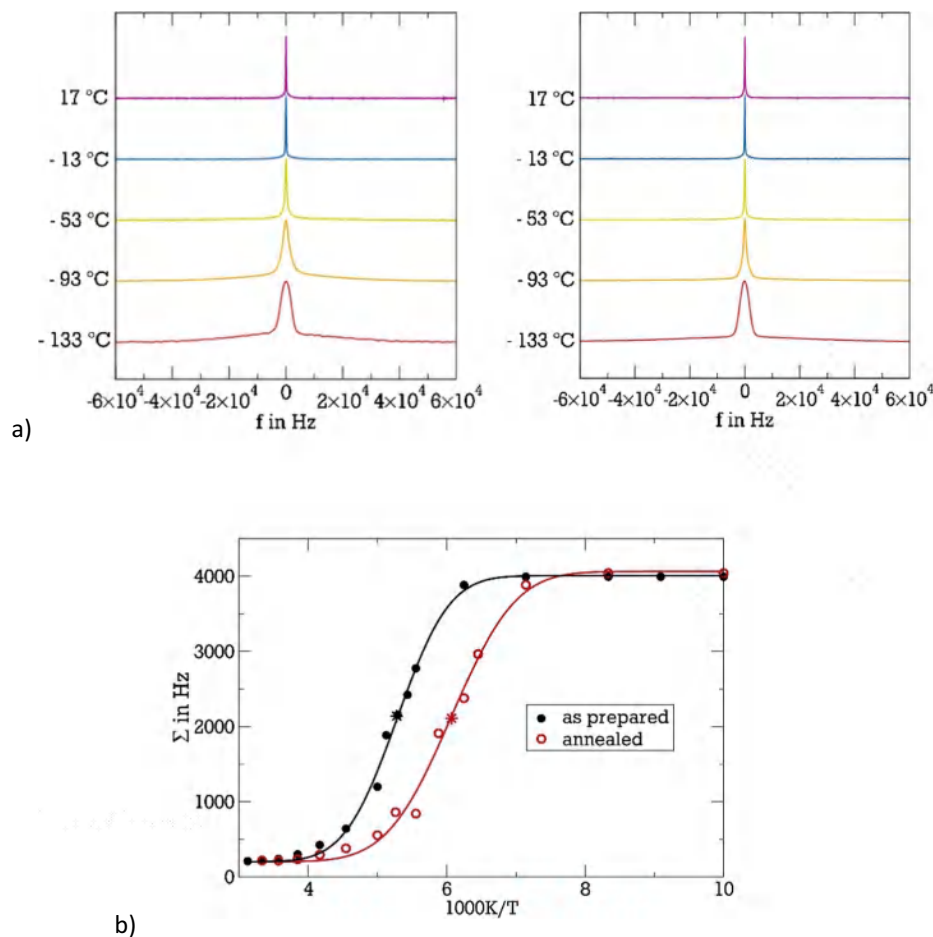
Fig. 3. a) Temperature-dependent ^{7}Li NMR spectra of the as prepared glass (left) and of a sample after a *single* annealing step (right). b) Temperature-dependent width of the central line in the ^{7}Li NMR spectra of the as-prepared glass and of the sample after a single annealing step. The temperature shift between the inflection points of both curves is about 25 K, as indicated by stars. The lines are guides to the eye.

activation energies. However, there is no indication of bimodal dynamics for either of the samples, which would result if ionic mobility was strongly altered in a precipitated phase. The line narrowing profile of the annealed sample is merely shifted by about 25 K to lower temperatures, confirming faster local Li$^+$ dynamics in the annealed sample as compared to the as-prepared glass. Strictly speaking, we expect that a minority fraction of a bimodal distribution is detectable in our line-shape analysis, if it amounts to at least 1–2%. In particular, a few percent of a highly mobile Li species would cause a clearly visible narrow line on top of the broad spectrum at temperatures just below the main line-shape transition. Smaller volume fractions of a precipitated phase could remain unobserved.

^{7}Li STE experiments provide straightforward access to Li ion jump motion in the milliseconds regime. In more detail, the ^{7}Li STE approach allows us to directly measure the correlation functions $F_2(t_m) \sim \langle \sin [\omega_{QP}(0)t_e] \cdot \sin [\omega_{QP}(t_m)t_e] \rangle$, relating the quadrupolar frequencies ω_{QP} during two short and fixed evolution times t_e that are separated by a longer and variable mixing time t_m [26,27,38]. Since the quadrupolar frequencies depend on the ionic environments, $F_2(t_m)$ decreases as a consequence of Li$^+$ jumps to neighbouring sites. Thus, $F_2(t_m)$ is a correlation function describing the depopulation of the Li$^+$ sites occupied at $t_m = 0$. Fig. 4 shows $F_2(t_m)$ for both samples. It is evident that the ^{7}Li STE decay of the as-prepared glass at $-133\,°C$ and of the annealed sample at $-113\,°C$ exhibit very similar characteristics. Interpolation with stretched exponential functions, $exp[-(t/\tau)^\beta]$, yields correlation times of $\tau \approx 0.02\,s$ and stretching parameters of $\beta \approx 0.7$. In this analysis, additional damping of the ^{7}Li STE decays due to spin relaxation
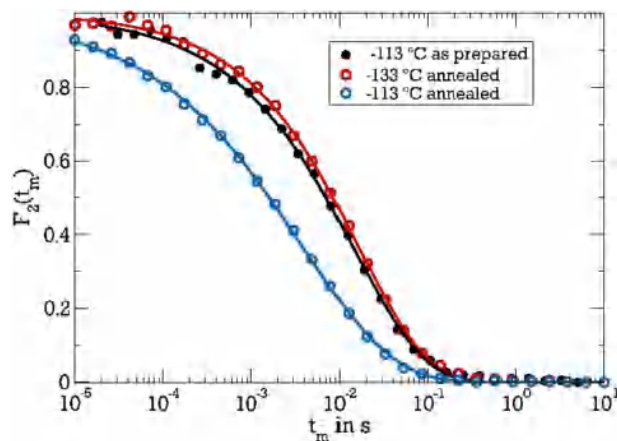

Fig. 4. Correlation functions $F_2(t_m)$ for the as-prepared glass (measured at $-113\,°C$) and for a sample after a single annealing step (measured at $-133\,°C$ and $-113\,°C$, respectively.) The lines are interpolations with stretched exponential functions, see text for details.

and spin diffusion [39] is minor. Thus, the observed temperature shift of 20 K further corroborates that annealing leads to an overall speedup of Li$^+$ dynamics. In harmony with the STE results, extrapolation of the measured electric conductivities, see Fig. 1, to the lower temperatures of the stimulated-echo study reveals that we expect comparable values of about $2 \cdot 10^{-5}\,mS \cdot cm^{-1}$ for the as prepared sample at $-113\,°C$ and

the annealed one at $-133\,°C$. On the other hand, comparison of the STE decays at $-113\,°C$ reveals that annealing speeds up Li ion jumps by almost an order of magnitude. For both samples, the stretched decays of $F_2(t_m)$ suggest appreciable dynamical heterogeneity. However, we do not observe bimodal decays for the annealed sample and, hence, the data yield no evidence for distinct jump rates in amorphous and crystalline regions. In other words, the ^{7}Li STE results indicate that all rather than a fraction of Li ions show enhanced dynamics after the single annealing step, confirming the results of the above line-shape analysis.

Finally, we use ^{7}Li SFG NMR to measure Li^+ self-diffusion coefficients. In these experiments, the ^{7}Li resonance frequencies depend on the Li position with respect to the applied magnetic field gradient. Thus, the resonance frequencies are no longer altered by next-neighbour jumps, but rather by long-range diffusion. To be more precise, our ^{7}Li SFG approach probes translational motion on length scales of about $1\,\mu m$. We perform STE experiments with fixed evolution time t_e and variable mixing time t_m to observe the resulting time dependence of the resonance frequencies. If free diffusion occurs, ^{7}Li self-diffusion coefficients D can be obtained by fitting these STE decays to single exponential functions $S(t_m) \sim e^{-(g\,\gamma\,t_e)^2 D t_m}$, where g denotes the field gradient and γ the gyromagnetic ratio. Thus, in analogy with the momentum transfer q in scattering experiments, the product $g\gamma t_e$ determines the length scale of the measurement. Fig. 5 shows ^{7}Li SFG STE decays obtained at $330\,K$ for the as-prepared glass and for the sample after a single annealing step. For a given evolution time t_e, the decay is faster by about a factor of two after annealing, indicating that such heat treatment speeds up Li diffusion. To analyse the validity of the free-diffusion model, we repeated the experiment for different values of t_e. We observed that the decays shift to shorter times when the evolution time and, hence, the spatial resolution is increased. Specifically, the SFG STE results for all used values of t_e are consistently described by global fits with a single diffusion coefficient D, when we consider minor additional spin-lattice relaxation damping for the shortest evolution time, $t_e = 20\,\mu s$, which is known from concomitant SLR measurements and fixed for the interpolation. These observations show that our approach yields reliable self-diffusion coefficients. At a temperature of $330\,K$, we find $D = 1.6 \cdot 10^{-12}\,m^2 \cdot s^{-1}$ for the as-prepared glass and $D = 4.5 \cdot 10^{-12}\,m^2 \cdot s^{-1}$ for the annealed sample. The corresponding Li^+ ion conductivities at $330\,K$ obtained from impedance spectroscopy are $\sigma_{Li^+} = 2.5\,mS \cdot cm^{-1}$ (as prepared) and $\sigma_{Li^+} = 7.7\,mS \cdot cm^{-1}$ (after single annealing step), respectively. From the mass density of the samples, $\rho = 2.15\,g \cdot cm^{-3}$, an overall number density of lithium ions of

Table 1
Fitting parameters obtained from PAL spectra of 0.33 LiI + 0.67 Li$_3$PS$_4$ glass as prepared and after a single annealing step at $180\,°C$.

Intensity I_1 (%)	Intensity I_2 (%)	Lifetime τ_1 (ps)	Lifetime τ_2 (ps)
As-prepared			
35.3 ± 3.6	64.8 ± 3.6	287 ± 12	428 ± 6
After single annealing step			
13.7 ± 1.0	86.3 ± 1.0	205 ± 13	405 ± 2

$N_V = 2.62 \cdot 10^{21}\,cm^{-3}$ is obtained. Now, we can use the Nernst-Einstein equation

$$\sigma_{Li^+} = \frac{N_V \cdot e^2}{k_B \cdot T \cdot H_R} \cdot D \tag{1}$$

to calculate the Haven ratio H_R. The obtained values of $H_R = 0.65$ for the as prepared glass and $H_R = 0.6$ for the sample after annealing are reasonable values for solid Li^+ ion conductors.

Altogether, our ^{7}Li NMR studies in homogeneous and inhomogeneous magnetic fields reveal that a single annealing step speeds up both next-neighbour jumps and long-range diffusion, in harmony with the findings of the above conductivity studies. None of the ^{7}Li NMR measurements provides evidence for bimodal dynamics in the annealed sample originating from faster ions in a crystalline phase or at interfaces and slower ions in the bulk amorphous phase, but the ^{7}Li NMR measurements provides strong evidence that the annealing leads to faster ion transport in the bulk amorphous phase.

In Table 1, we give the relative intensities and lifetimes obtained for the two components in the positron-annihilation lifetime (PAL) spectra of an as-prepared sample and of a sample after a single annealing step. The main influence of the annealing on the PAL spectra is the shortening of lifetime τ_1 from 287 ps to 205 ps and the increase of the intensity ratio I_2/I_1 from 1.8 to 6.3. Such two-component PAL spectra can often be interpreted in the framework of a model with positron capture by a single type of defects [40]. The parameters in such a model are the annihilation rate of the positrons in a defect-free material λ_b, the trapping rate of the positrons by the defects κ_D, and the positron annihilation rate at the defects λ_D. With these parameters, the lifetimes τ_1 and τ_2 and the intensity ratio I_2/I_1 can be expressed as:

$$\tau_1 = \frac{1}{\lambda_B + \kappa_D} \tag{2}$$

$$\tau_2 = \frac{1}{\lambda_D} \tag{3}$$

$$\frac{I_2}{I_1} = \frac{\kappa_D}{\lambda_B - \lambda_D} \tag{4}$$

Combining these equations, the annihilation rate in a defect-free material λ_b can be written as:

$$\lambda_B = \frac{1}{\tau_B} = \frac{I_1}{\tau_1} + \frac{I_2}{\tau_2} \tag{5}$$

τ_B is the positron bulk lifetime in the defect-free material. From Eq. (5), we obtain $\tau_B = 364\,ps$ for the as-prepared material and $\tau_B = 357\,ps$ after the one-step annealing. Thus, the bulk lifetime is more or less unaffected by the annealing. The positron annihilation rate at defects $\lambda_D = 1/\tau_2$ increases slightly after annealing, but the main effect of the annealing is the decrease of τ_1 and the increase of the intensity ratio I_2/I_1. Considering Eqs. (2) and (4), this points to a strong increase of the defect trapping rate κ_D during annealing. From these equations we obtain an average value of $\kappa_D = 7.5 \cdot 10^{-4}\,ps^{-1}$ for the as-prepared sample and $\kappa_D = 2.1 \cdot 10^{-3}\,ps^{-1}$ after one-step annealing. Since the defect trapping rate is proportional to the defect concentration [40], these results provide evidence for an increase of the defect concentration by a factor of about 2.8 during annealing. Information on the

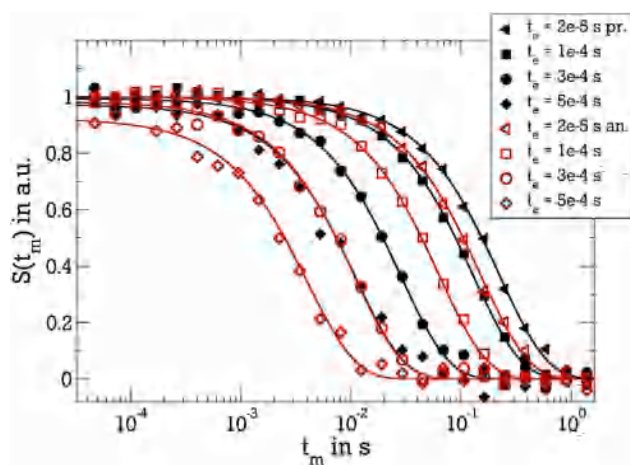**Fig. 5.** Static-field-gradient diffusion measurements at $T = 330\,K$ on the as-prepared sample (full black symbols) and on the annealed sample (open red symbols). Diffusion coefficients were obtained from STE decays $S(t_m)$ for various evolution times t_m. The solid lines are global fits with the model of free diffusion, see text for details. (For interpretation of the references to color in this figure legend, the reader is referred to the web version of this article.)

defect type can be obtained from the ratio τ_B/τ_2, which is 1.17 for the as-prepared glass and 1.12 for the annealed sample. Such low values point to monovacancies as defects [40].

Thus, the combination of the electrochemical impedance, ^{7}Li NMR, PAL spectroscopy gives strong indication that the enhancement of the Li^+ ion conductivity in the bulk amorphous phase is caused by a strong increase in the concentration of monovacancies, which act as stepping stones for the hopping transport of the Li^+ ions. Here, it is important to note that there is no general definition of vacancies in amorphous materials, in contrast to crystalline material with well-defined lattice sites. However, MD simulations of Li^+ ion conducting glasses have revealed well-defined empty Li^+ sites in the amorphous structure [41–43]. The ratio of these empty sites to the sites filled with Li^+ ions was found to be about 0.1, i.e. there are only few more Li^+ sites than mobile Li^+ ions. The low fraction of empty sites should thus be a limiting factor for the long-range ion transport. Consequently, increasing the number of such empty sites by a factor of 2.8 during the annealing should indeed lead to a substantial increase of the ionic conductivity.

4. Conclusions

We have demonstrated that a simple one-step annealing of amorphous $0.33 \, LiI + 0.67 \, Li_3PS_4$ at $180\,°C$ increases the Li^+ ion conductivity from about $0.8 \, mS \cdot cm^{-1}$ to $6.5 \, mS \cdot cm^{-1}$. After this single annealing step, the sample is still mostly amorphous. By combining the electrochemical impedance, ^{7}Li NMR and PAL spectroscopy, we give evidence that the conductivity enhancement is neither based on highly conductive crystallites nor on fast interfacial ion transport, but is caused by an annealing-induced formation of monovacancies in the bulk amorphous phase, which act as stepping stones for fast Li^+ ion transport. This scenario is plausible from a theoretical point of view, since molecular dynamics simulations of Li^+ ion conducting glasses have revealed that the number of empty Li^+ sites in the amorphous matrix is much smaller than the number of mobile Li^+ ions. The low fraction of empty Li^+ sites is thus a limiting factor for fast Li^+ ion transport, so that an annealing-induced formation of monovacancies, which are able to accommodate Li^+ ions, should lead to a significant conductivity enhancement.

Acknowledgment

References

[1] Y. Kato, T. Saito, H. Iba, M. Hirayama, A. Mitsui, M. Yonemura, R. Suzuki, S.H. KotaKanno, High-power all-solid-state batteries using sulfide superionic conductors, Nat. Energy 1 (2016) 16030, , https://doi.org/10.1038/nenergy.2016.30.

[2] Y. Kato, K. Kawamoto, R. Kanno, M. Hirayama, Discharge performance of all-solid-state battery using a lithium superionic conductor Li10GeP2S12, Electrochemistry 80 (2012) 749–751, https://doi.org/10.5796/electrochemistry.80.749.

[3] M. Tatsumisago, F. Mizuno, A. Hayashi, All-solid-state lithium secondary batteries using sulfide-based glass-ceramic electrolytes, J. Power Sources 159 (2006) 193–199, https://doi.org/10.1016/j.jpowsour.2006.04.037.

[4] D. Liu, W. Zhu, Z. Feng, A. Guerfi, A. Vijh, K. Zaghib, Recent progress in sulfide-based solid electrolytes for Li-ion batteries, Mater. Sci. Eng. B Solid-State Mater. Adv. Technol. 213 (2016) 169–176, https://doi.org/10.1016/j.mseb.2016.03.005.

[5] P. Bron, S. Dehnen, B. Roling, Li 10 Si 0.3 Sn 0.7 P 2 S 12 – a low-cost and low-grain-boundary-resistance lithium superionic conductor, J. Power Sources 329 (2016) 530–535, https://doi.org/10.1016/j.jpowsour.2016.08.115.

[6] J. Janek, W.G. Zeier, A solid future for battery development, Nat. Energy 1 (2016) 1–4, https://doi.org/10.1038/nenergy.2016.141.

[7] N. Kamaya, Y. Yamakawa, S. Hama, A. Mitsui, M. Hirayama, Y. Kato, R. Kanno, T. Kamiyama, M. Yonemura, K. Kawamoto, K. Homma, A lithium superionic conductor, Nat. Mater. 10 (2011) 682–686, https://doi.org/10.1038/nmat3066.

[8] M.R. Busche, W. Zhang, D.A. Weber, S. Wenzel, S.J. Sedlmaier, Y. Schneider, D. Walter, T. Leichtweiss, L.F. Nazar, D. Houtarde, C. Dietrich, J. Janek, D. Schröder, H. Weigand, In situ monitoring of fast Li-ion conductor Li 7 P 3 S 11

[9] crystallization inside a hot-press setup, Chem. Mater. 28 (2016) 6152–6165, https://doi.org/10.1021/acs.chemmater.6b02163.

[9] J.C. Bachman, S. Muy, A. Grimaud, S. Lupart, Y. Shao-Horn, S.F. Lux, L. Giordano, N. Pour, H.-H. Chang, O. Paschos, F. Maglia, P. Lamp, Inorganic solid-state electrolytes for lithium batteries: mechanisms and properties governing ion conduction, Chem. Rev. 116 (2015) 140–162, https://doi.org/10.1021/acs.chemrev.5b00563.

[10] F. Zheng, M. Kotobuki, S. Song, M.O. Lai, L. Lu, Review on solid electrolytes for all-solid-state lithium-ion batteries, J. Power Sources 389 (2018) 198–213, https://doi.org/10.1016/j.jpowsour.2018.04.022.

[11] J. Trevey, J.S. Jang, Y.S. Jung, C.R. Stoldt, S.-H. Lee, Glass–ceramic Li2S–P2S5 electrolytes prepared by a single step ball billing process and their application for all-solid-state lithium–ion batteries, Electrochem. Commun. 11 (2009) 1830–1833, https://doi.org/10.1016/j.elecom.2009.07.028.

[12] A. Pradel, M. Ribes, Lithium chalcogenide conductive glasses, Mater. Chem. Phys. 23 (1989) 121–142, https://doi.org/10.1016/0254-0584(89)90021-7.

[13] R. Mercier, J.P. Malugani, B. Fahys, G. Robert, Superionic conduction in Li2S - P2S5 - LiI - glasses, Solid State Ionics 5 (1981) 663–666, https://doi.org/10.1016/0167-2738(81)90341-6.

[14] S. Ujiie, A. Hayashi, M. Tatsumisago, Preparation and ionic conductivity of (100-x) (0.8Li2S·0. 2P2S5)·xLiI glass-ceramic electrolytes, J. Solid State Electrochem. 17 (2013) 675–680, https://doi.org/10.1007/s10008-012-1900-7.

[15] E. Rangasamy, Z. Liu, M. Gobet, K. Pilar, G. Sahu, W. Zhou, H. Wu, S. Greenbaum, C. Liang, An iodide-based Li7P2S8I superionic conductor, J. Am. Chem. Soc. 137 (2015) 1384–1387, https://doi.org/10.1021/ja508723m.

[16] S. Ujiie, A. Hayashi, M. Tatsumisago, Structure, ionic conductivity and electrochemical stability of Li 2S-P 2S 5-LiI glass and glass-ceramic electrolytes, Solid State Ionics 211 (2012) 42–45, https://doi.org/10.1016/j.ssi.2012.01.017.

[17] P. Bron, B. Roling, S. Dehnen, Impedance characterization reveals mixed conducting interphases between sulfidic superionic conductors and lithium metal electrodes, J. Power Sources 352 (2017) 127–134, https://doi.org/10.1016/j.jpowsour.2017.03.103.

[18] F. Han, J. Yue, X. Zhu, C. Wang, Suppressing Li dendrite formation in Li2S-P2S5 solid electrolyte by LiI incorporation, Adv. Energy Mater. 8 (2018) 2–7, https://doi.org/10.1002/aenm.201703644.

[19] Y. Zhu, X. He, Y. Mo, Origin of outstanding stability in the lithium solid electrolyte materials: insights from thermodynamic analyses based on first-principles calculations, ACS Appl. Mater. Interfaces 7 (2015) 23685–23693, https://doi.org/10.1021/acsami.5b07517.

[20] M. Tatsumisago, A. Hayashi, Superionic glasses and glass-ceramics in the Li 2S-P 2S 5 system for all-solid-state lithium secondary batteries, Solid State Ionics 225 (2012) 342–345, https://doi.org/10.1016/j.ssi.2012.03.013.

[21] F. Mizuno, A. Hayashi, K. Tadanaga, M. Tatsumisago, New, highly ion-conductive crystals precipitated from Li 2S-P2S5 glasses, Adv. Mater. 17 (2005) 918–921, https://doi.org/10.1002/adma.200401286.

[22] Y. Seino, T. Ota, K. Takada, A. Hayashi, M. Tatsumisago, A sulphide lithium super ion conductor is superior to liquid ion conductors for use in rechargeable batteries, Energy Environ. Sci. 7 (2014) 627–631, https://doi.org/10.1039/c3ee41655k.

[23] A. Hayashi, S. Hama, T. Minami, M. Tatsumisago, Formation of superionic crystals from mechanically milled Li2S-P2S5glasses, Electrochem. Commun. 5 (2003) 111–114, https://doi.org/10.1016/S1388-2481(02)00555-6.

[24] H. Tsukasaki, S. Mori, S. Shiotani, H. Yamamura, Ionic conductivity and crystallization process in the Li2S–P2S5 glass electrolyte, Solid State Ionics 317 (2018) 122–126, https://doi.org/10.1016/j.ssi.2018.01.010.

[25] S. Shiotani, K. Ohara, H. Tsukasaki, R. Kanno, S. Mori, Pair distribution function analysis of sulfide glassy electrolytes for all-solid-state batteries: understanding the improvement of ionic conductivity under annealing condition, Sci. Rep. 7 (2017) 1–7, https://doi.org/10.1038/s41598-017-07086-y.

[26] R. Böhmer, K.R. Jeffrey, M. Vogel, Solid-state Li NMR with applications to the translational dynamics in ion conductors, Prog. Nucl. Magn. Reson. Spectrosc. 50 (2007) 87–174, https://doi.org/10.1016/j.pnmrs.2006.12.001.

[27] R. Böhmer, M. Storek, M. Vogel, NMR studies of ionic dynamics in solids, In: Modern Methods in Solid-State NMR 5 (2018) 193–232, https://doi.org/10.1039/9781788010467-00193.

[28] B. Geil, Measurement of translational molecular diffusion using ultrahigh magnetic field gradient NMR, Concepts Magn. Reson. 10 (1998) 299–321, https://doi.org/10.1002/(SICI)1099-0534(1998)10:5 < 299::AID-CMR3 > 3.0.CO;2-S.

[29] O. Hauenstein, M.M. Rahman, M. Elsayed, R. Krause-Rehberg, S. Agarwal, V. Abetz, A. Greiner, Biobased polycarbonate as a gas separation membrane and "breathing glass" for energy saving applications, Adv. Mater. Technol. 2 (2017), https://doi.org/10.1002/admt.201700026.

[30] F. Lotter, U. Muehle, M. Elsayed, A.M. Ibrahim, T. Schubert, R. Krause-Rehberg, B. Kieback, T.E.M. Staab, Precipitation behavior in high-purity aluminium alloys with trace elements – the role of quenched-in vacancies, Phys. Status Solidi A. 215 (2018), https://doi.org/10.1002/pssa.201800375 (18003751–11).

[31] J. Kansy, Microcomputer program for analysis of positron annihilation lifetime spectra, Nucl. Instruments Methods Phys. Res. A 374 (1996) 235–244.

[32] B. Hirschorn, M.E. Orazem, B. Tribollet, V. Vivier, I. Frateur, M. Musiani, Determination of effective capacitance and film thickness from constant-phase-element parameters, Electrochim. Acta 55 (2010) 6218–6227, https://doi.org/10.1016/j.electacta.2009.10.065.

[33] J.T.S. Irvine, D.C. Sinclair, A.R. West, Electroceramics: characterisation by impedance spectroscopy, Adv. Mater. 2 (1990) 132–138.

[34] S.J. Sedlmaier, S. Indris, C. Dietrich, M. Yavuz, C. Dräger, F. Von Seggern, H. Sommer, J. Janek, Li4PS4I: a Li + superionic conductor synthesized by a solvent-based soft chemistry approach, Chem. Mater. 29 (2017) 1830–1835, https://doi.org/10.1021/acs.chemmater.7b00013.

[35] K. Homma, M. Yonemura, T. Kobayashi, M. Nagao, M. Hirayama, R. Kanno, Crystal structure and phase transitions of the lithium ionic conductor Li3PS4, Solid State Ionics 182 (2011) 53–58, https://doi.org/10.1016/j.ssi.2010.10.001.

[36] K. Hayamizu, Y. Aihara, T. Watanabe, T. Yamada, S. Ito, N. Machida, NMR studies on lithium ion migration in sulfide-based conductors, amorphous and crystalline Li3PS4, Solid State Ionics 285 (2016) 51–58, https://doi.org/10.1016/j.ssi.2015.06.016.

[37] S. Adams, K. Hariharan, J. Maier, Interface effect on the silver ion conductivity during the crystallization of AgIAg2OV2O5 glasses, Solid State Ionics 75 (1995) 193–201, https://doi.org/10.1016/0167-2738(94)00219-I.

[38] M. Wilkening, P. Heitjans, From micro to macro: access to long-range Li+ diffusion parameters in solids via microscopic 6,7Li spin-alignment echo NMR spectroscopy, ChemPhysChem 13 (2012) 53–65, https://doi.org/10.1002/cphc.201100580.

[39] S. Faske, H. Eckert, M. Vogel, 6Li and 7Li NMR line-shape and stimulated-echo studies of lithium ionic hopping in LiPO3 glass, Phys. Rev. B 77 (2008) 104301, , https://doi.org/10.1103/PhysRevB.77.104301.

[40] R. Krause-Rehberg, H.S. Leipner, Positron Annihilation in Semiconductors, (1998).

[41] H. Lammert, M. Kunow, A. Heuer, Complete identification of alkali sites in ion conducting lithium silicate glasses: a computer study of ion dynamics, Phys. Rev. Lett. 90 (2003) 2159011–2159014, https://doi.org/10.1103/PhysRevLett.90.215901.

[42] H. Lammert, A. Heuer, Simplified interpretation of transport in disordered inorganic ion conductors from vacancy dynamics, Phys. Rev. Lett. 104 (2010) 1–4, https://doi.org/10.1103/PhysRevLett.104.125901.

[43] M. Vogel, Identification of lithium sites in a model of LiPO3 glass: effects of the local structure and energy landscape on ionic jump dynamics, Phys. Rev. B 70 (2004) 094302, , https://doi.org/10.1103/PhysRevB.70.094302.